ON THE QUALITY OF A RELAXATIONAL METHOD FOR 3D GRAVITY INVERSION

Neki FRASHËRI and Salvatore BUSHATI
Albanian Academy of Sciences

_____

ABSTRACT

The quality of 3D inversion of gravity anomalies in parallel computer systems is in the present paper reported. The 3D geosection distribution of mass density has been updated step by step using the relaxation iterative principle for the minimal least squares error of generated anomaly compared with the observed anomaly. Cases of multi-body geosections are analysed and the results show that the separation ability of the algorithm depends on the distance of real bodies.
Keywords: 3D gravity inversion, relaxation method

1. INTRODUCTION

Holographic principle cannot be fully applied for the traditional inversion of gravity anomalies because the data of the field measured were obtained from a small region of the 3D geosection boundary, in the ground surface, that represents in average the 1/6 of the whole boundary surface of geosection. In addition, calculations were based on the simple formula of gravity potential c*m/r that makes the inversion solution very common and similar anomalies may be obtained from different masses m at different depths (Hadamard 1902; Lowrie 2007).

Many methods have been applied to tackle the 2D and 3D inversion (Sen and Stoffa 1995; Silva *et. al*., 2000; Xiaobing 2009; Shamsipour *et al*., 2010; Wellmann *et al*., 2010; Wilson *et al*., 2011; Hou Zhen-Long *et al*., 2019). Some methods consider regular prismatic or convex 3D bodies. To cope with the lack of uniqueness, the solution probabilistic components were added to the inversion processes. Finally, the parallel systems were used to speed-up calculations within a reasonable runtime. Nevertheless, one of the most typical problems of the inversion in case of multi-body geosections is the generation of false in-depth "bridges" between the bodies (Zhdanov *et al*., 2010; Wilson *et al*., 2011) and lack of contrast between different rocky bodies.

We used a relaxation iterative principle to update step by step the 3D geosection distribution of mass density for the minimal least squares error of

generated anomaly compared with the observed anomaly. The present paper reports the inversion of 3D geosections with three and four vertical prismatic bodies, placing them at two different distances from each other. Significant improvement of the inverted geosection when bodies were placed at a certain distance from each other was reported.

The present study has been carried out in the framework of European actions and supported by parallel computing capacities offered by related regional infrastructure (see acknowledgment for details).

2. MATERIALS AND METHODS

The relaxation method technique was employed based on the CLEAN algorithm, first raised by Hogbom in 1970s to improve the image quality of single radio interferometer in astronomy. The 3D geosection was split into 3D small cells regular mesh. The relaxation principle was applied to generate step by step the discretized 3D geosection adding small "quanta" updates of mass density in one specific cell during every main iteration. The specific cell to be modified is selected scanning the whole 3D mesh, comparing the elementary anomaly of each cell with the shape of residual global anomaly, selecting the best one, and subtracting its effect from the residual anomaly. The next main iteration uses the reduced (i.e. relaxed) global anomaly as a goal to be reached. Farther information including analysis of scalability of runtime in parallel systems could be found in (Frashëri and Bushati 2012; Frashëri *et al*., 2013; Frashëri and Atanassov 2019).

Mathematically, the field observed data is represented by 2D points matrix G of dimensions NsNt, while the digitized 3D geosection using 3D nodes matrix M of dimensions NiNjNk.

Simple logic leads to the complexity of our iterative algorithm O (N^8) for the same spatial extension of the geosection, where N is the linear average dimension of used 2D and 3D matrices representing the spatial resolution of the geosection. Main iterations are composed of N^3N^2 elementary iterations, each of them calculates the impact of one 3D mesh cell at one of 2D surface measurement points, i.e. the order O (N^5). The additional order O(N^3) is result of the fact that increasing N implies reduction of 3D volume of cells and the need to increase in the same order the number of main iterations to obtain the same mass distribution.

The 3D geosection mesh was scanned to identify the updateable 3D mesh cell in each main iteration. Each cell of the mesh (node M_{ijk}) has its gravity impact A_{st} is calculated (as elementary iteration) for each surface point (s,t) where the anomaly G_{st} is measured. The weighted least squares error was used as metrics to compare shapes of elementary anomalies (2D matrix A)

generated by the 3D mesh cell (i,j,k), and that of the residual global anomaly (matrix G):

$$Err_{ijk} = \sum_{st} w_{st} (G_{st} - c * A_{st} - b_x x_{st} - b_y y_{st} - d)^2$$

(1)

where: W is the 2D array of weights, c is the rock mass to be concentrated in the cell (i, j, k), and bx, by and d are the coefficients of the linear trend of the residual anomaly over the cell.

The linear trend was subtracted from the residual anomaly to avoid anomalous impact of the regional rock masses (case of multi-bodies geosection) while considering the effect of a localized anomaly created by a single cuboid in the value of error Errijk.

Weights wst were used to increase the weight of elementary anomaly central values in calculation of the error Errijk, and to avoid peripheral values that tent towards zero.

The weights array W was calculated using the values of elementary anomalies:

$$w_{st} = \frac{A_{st}^{wc}}{\frac{\sum_{st} A_{st}^{wc}}{count}}$$

(2)

where: wc is a constant defining the power of weights, and count is the number of counted elementary anomaly values (count = N^2 in our case).

In each main iteration, the best fit cell mass is increased or decreased with the predefined quanta of mass density, depending on the sign of constant c (equation (1)). After the contribution A of the elementary anomaly is subtracted from the residual observed one G, the summation of absolute values from formula (2) was calculated and considered as the inversion error for the main iteration in course:

$$Err = \frac{\sum_{st} |G_{st}|}{N^2}$$

(3)

Iterative process could not end unless the best fit update of selected mesh cell (constant c in equation (1)) is less than half of predefined mass density quanta and the average error of last iterations experienced an increase.

The algorithm as function of mesh resolution is tested for geosections with one, two, three and four vertical prismatic bodies. The used geosections are 4,000m*4,000m*2,000m in size, with mesh resolution 400m, 200m and

100m. The rectangular prismatic bodies of 400m*400m*1,600m in size could be found from the bottom of geosection up to 400m deep, under the ground surface. The distance between bodies is 1,414m or 2,000m depending on their reciprocal positions (ortogonal or diagonal, Figure 1).
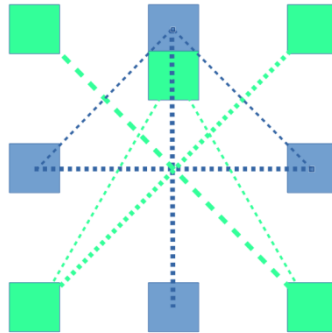
Fig. 4: Top view of prismatic bodies reciprocal position: blue – orthogonal case with distances 2000 and 1414 m for 1-4 body sections; green – diagonal case with distances 2000 m for 3 and 4 body sections.

3. RESULTS ANALYSIS

Figure 2 depicts the observed gravity anomaly calculated in all four cases of bodies position in the geosection.

single body

single body calculated anomaly

two-body section

three body orthogonal section

two-body calculated anomaly

three-body orthogonal calculated anomaly

four body orthogonal section

four body orthogonal calculated anomaly
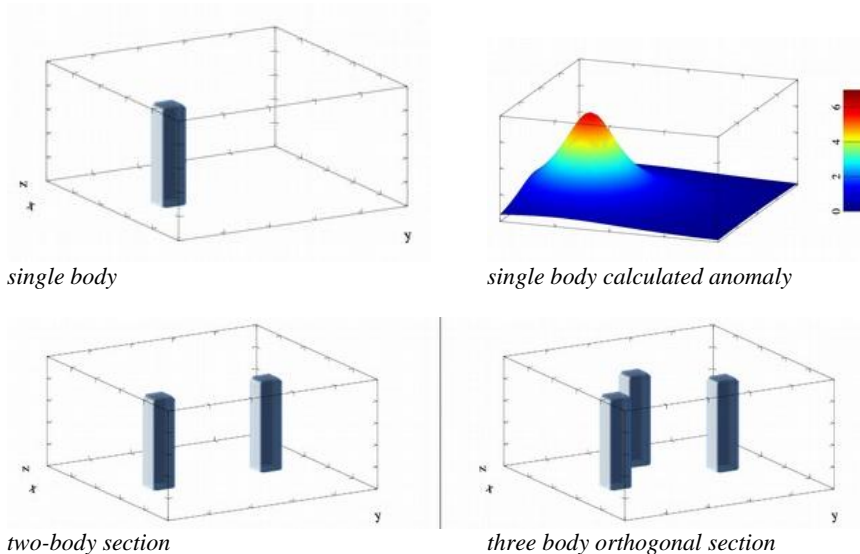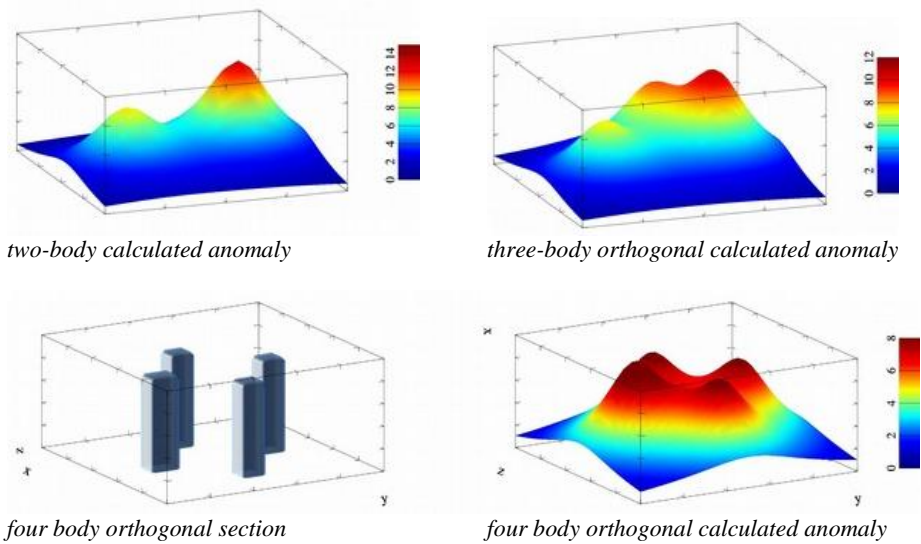
Fig. 2: Four types of 3D geosections and their respective gravity anomalies.

We repeated the calculations with different values of the weight power constant (formula (3)). Error dependence upon the value of weight power constant is in Figure 3 depicted.
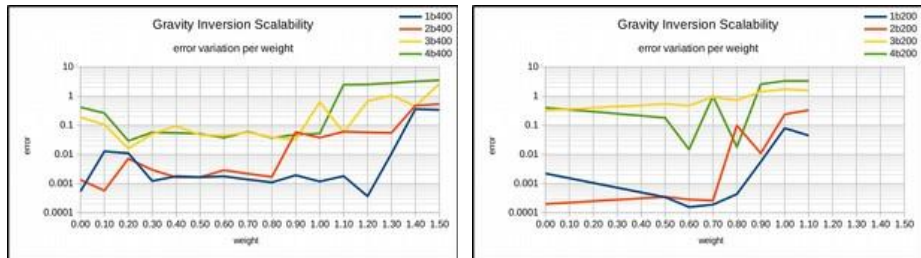
Fig. 3: Error dependence upon weight power for mesh with resolution 400m (left) and 200m (right).

Oscillations of error, especially for the geosection with four bodies, showed the need for several runs of software for the same model in order to define the best weight power value. In our final tests we used the power value of 0.5.

Figure 4 depicts the acceptable inversion errors for cases of 3D geosections with one and two bodies and significantly increased inversion errors for cases of 3D geosections with three and four bodies.

single body inversion with negative relative densities and related error

two-body inversion with negative relative densities and related error

three-body orthogonal case inversion with negative relative densities and related error

four-body orthogonal case inversion with negative relative densities and related error
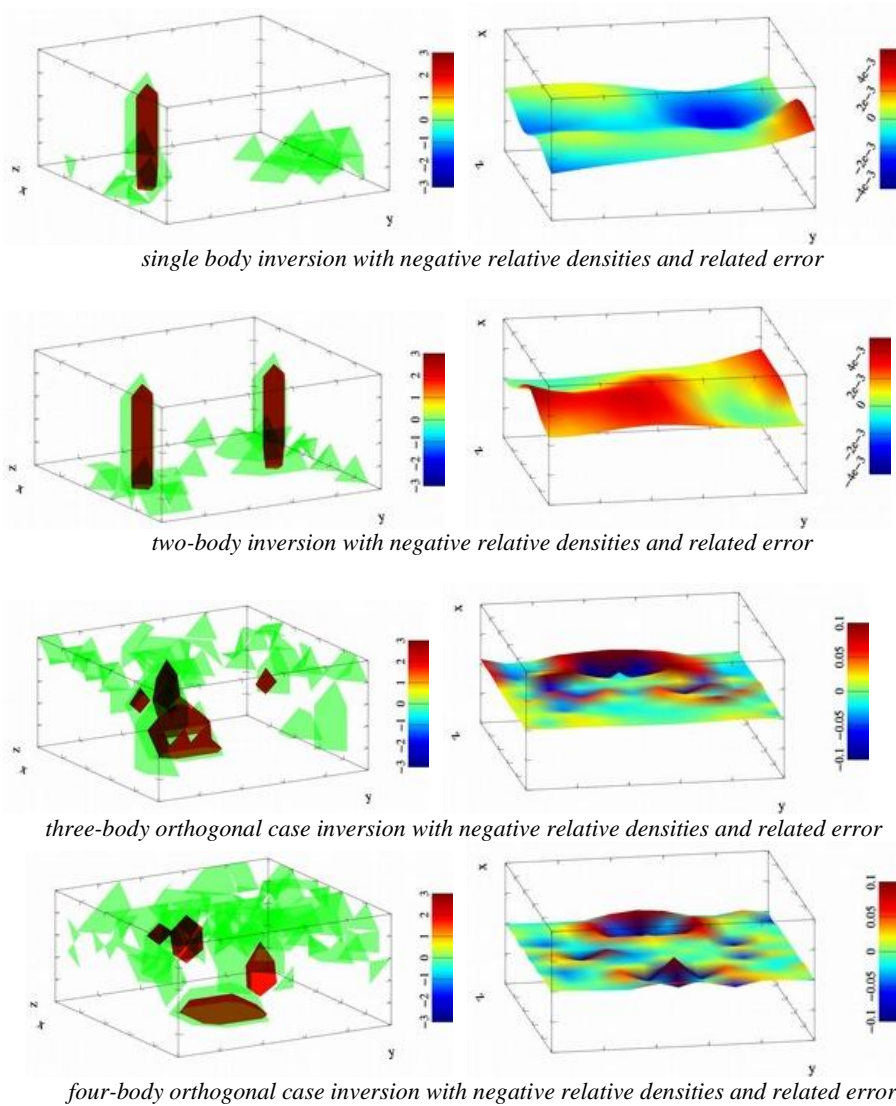
Fig. 4: Error of inversion for different geosections with one, two, three and four bodies.

Inversion for single and two-body geosections resulted of good quality, with bodies clearly delineated in contrast with surrounding environment. Figure 5 depicts the orthogonal view of these cases (only positive relative densities are accepted).
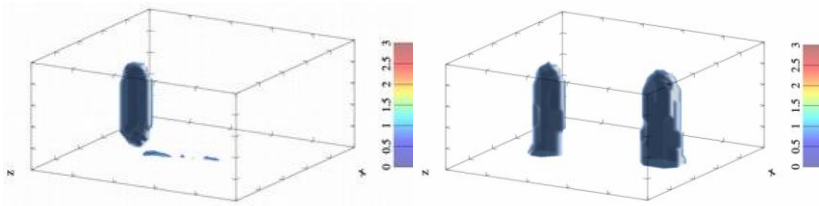
Fig. 5: Inverted geosections for one and two bodies: single body case – left, and two body case – right.

In contrast, the inversion for three- and four-bodies geosections resulted of low quality, with deformed bodies and additional false masses, always clearly delineated (Figure 6).

inversion of three and four body orthogonal

side view of inversion for three body orthogonal section
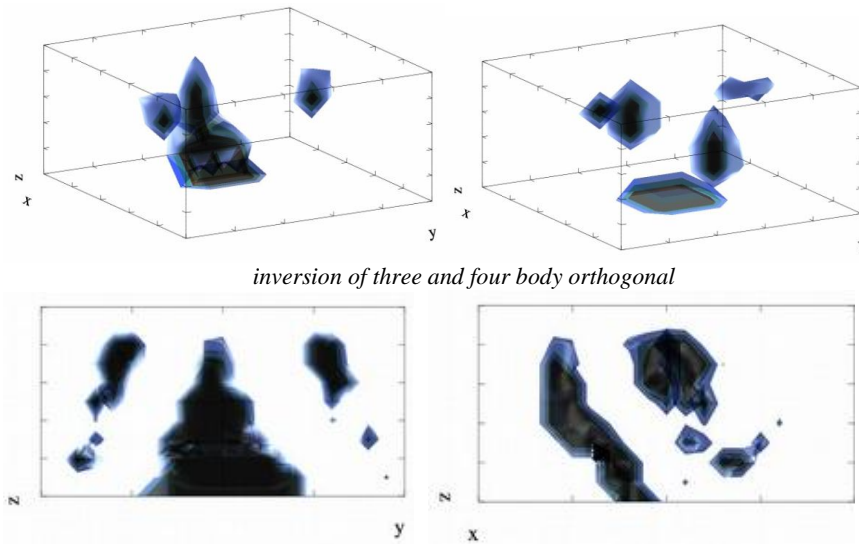
Fig. 6: Inverted geosections for three and four bodies.

Finally, two tests were made accepting only positive changes of mass density for geosections of resolution 200m with three and four bodies (inversion results shown in Fig. 1-6). The error was improved ten times with less increase in iterations and runtime, and the respective values are in the Table 1 reported. Improvement of the error varied from 5 to 10 times for an increase of iterations and runtime up to 50%.

Table 1. Change of inversion quality for positive updates of mass density

Geosection	Error	Iterations	Runtime (seconds)
3 bodies	0.9355 => 0.0854	2474 => 3407	447.31 => 597.77
4 bodies	0.9916 => 0.1714	42885 => 4741	775.22 => 794.15

We hypothesized that degeneration of solution for three and four bodies relates to their distances from each other. When the distance between bodies was increased to 2000m (case diagonal), for three- and four-bodies geosections, the generated individual anomalies were more clearly separated from each other (Figure 7).

three-body diagonal section   three-body diagonal calculated anomaly

four-body diagonal section   four-body diagonal calculated anomaly
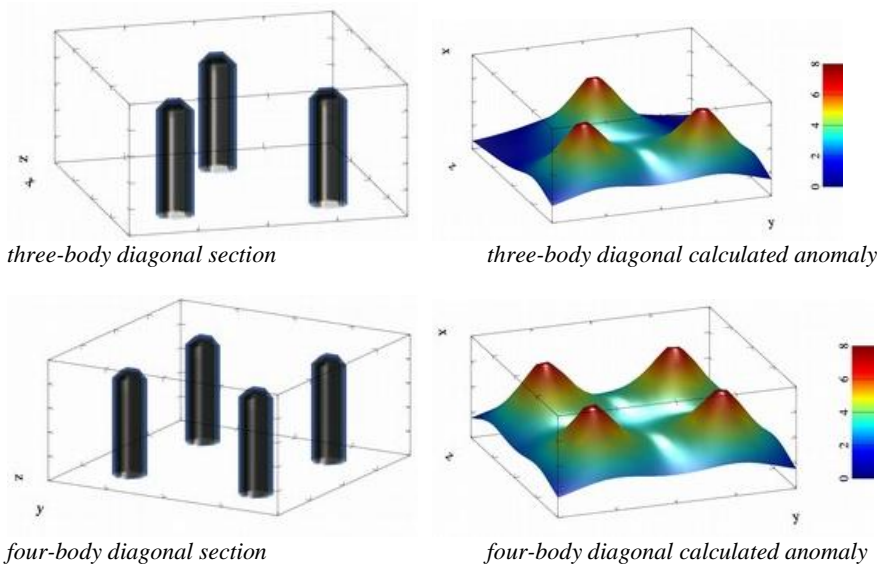
Fig. 7: 3D geosections with three and four more distant from each other bodies and respective gravity anomalies

Inversion in these cases resulted much better, with deformed bodies situated in right places compared with original geosections; additional false bodies are still present but smaller in size (Figure 8):

Improved inversion of three body (left) and four body (right) diagonal geosections.

four body diagonal case inversion – side view   *four body diagonal case inversion – top view*
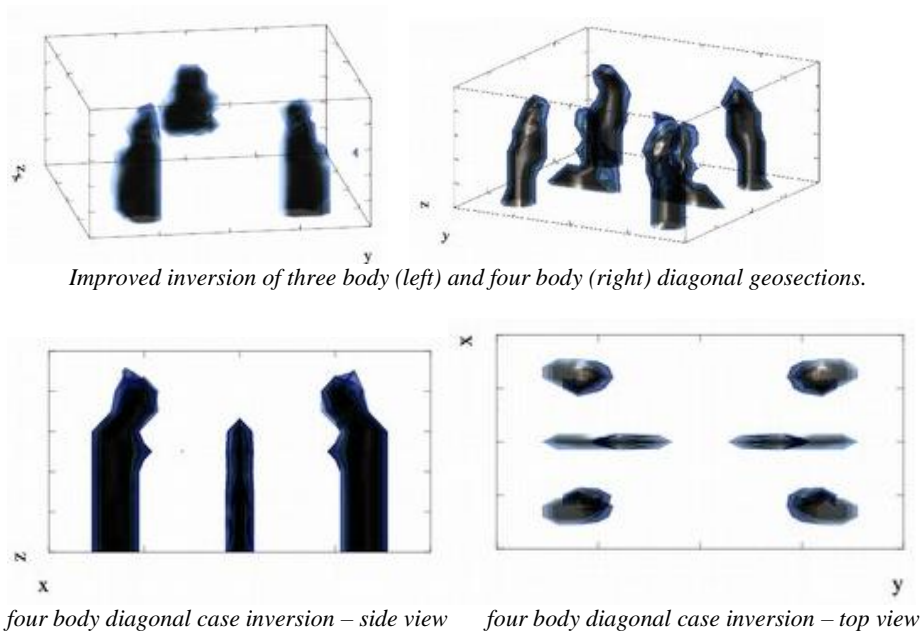
Fig. 8: Views of improved inverted geosections with three and four bodies

4. CONCLUSIONS

Complexity of the algorithm resulted $O(N^8)$ with parallel calculations effectivity over 90%, leading to significant increase of runtime when resolution of models increased suitably for engineering purposes, requesting even days when running in thousands cores. Extrapolated runtime for the inversion of a geosection 4km*4km*2km with resolution 25m resulted 26 days in a HPC system as Avitohol (Frashëri and Atanassov 2019).

The algorithm depends on parameters least squares weights power and mass density quanta. Variation of inversion quality resulted complicated and difficult to be evaluated a-priori; requesting several runs of the software using different parameter values in order to pick up the best possible error.

Inversion quality resulted quite well for the geosections with one and two bodies, while degraded for three and four bodies. In latter case the distance between bodies resulted to have significant negative impact in the quality of inversion, leading to the deformation of bodies and introduction of false bodies; inversion quality was improved when bodies situated farther from each other.

ACKNOWLEDGMENTS

REFERENCES

Frashëri N, Atanassov E. 2019. Scalability of 3D relaxational gravity inversion in HPC Avitohol. In *Ultrascale Computing Systems*, Eds. J.Carretero, E.Jeannot and A. Zomaya, IET (The Institution of Enginering and Technology) Professional Applications of Computing Series 24.

Frashëri N, Bushati S, Frashëri A. 2013. A parallel processing algorithm for gravity inversion. European Geosciences Union General Assembly EGU'2013 Vienna 7-12 April; 2013. Available from: https://meetingorganizer.copernicus.org/EGU2013/EGU2013-8739-1.pdf

Frashëri N, Bushati S. 2012. An algorithm for gravity anomaly inversion in HPC. SCPE: *Scalable Computing: Practice and Experience*. **13(2):**51–69.

Högbom JA. 1974. Aperture synthesis with a non-regular distribution of interferometer baselines. *Astrophys Suppl*; 15:417.

Hadamard J. 1902. Sur les Problemes aux Derivees Partielles et leur Signification Physique. Bull Princeton University. 13, 49-52.

Hou Zhen-Long, Huang Da-Nian, Wang En-De, Cheng Hao. 2019. 3D density inversion of gravity gradiometry data with a multilevel hybrid parallel algorithm. *Applied Geophysics* 16(1). June 2019.

Lowrie W. 2007. Fundamentals of Geophysics. Cambridge University Press.

Sen M, Stoffa P. 1995. Global Optimization Methods in Geophysical Inversion. Elsevier Science B.V.

Shamsipour P, Chouteau M, Marcotte D, Keating P. 2010. 3D stochastic inversion of borehole and surface gravity data using geostatistics. *EGM International Workshop on Adding new Value to Electromagnetic, Gravity and Magnetic Methods for Exploration*, Capri, Italy, April 11-14. Available from: http://www.eageseg.org/data/egm2010/Sessione%20C/ Oral%20papers/COP06.pdf.

Silva J, Medeiros WE, Barbosa VCF. 2000. Gravity inversion using convexity constraint. *Geophysics*; 65(1):102–112.

Wellmann FJ, Horowitz FG, Schill E, Klaus Regenauer-Lieb. 2010. Towards incorporating uncertainty of structural data in 3D geological inversion. Elsevier Tectonophysics TECTO-124902.

Wilson G, Cuma M, Zhdanov MS. 2011. Massively parallel 3D inversion of gravity and gravity gradiometry data. PREVIEW, *The Magazine of the Australian Society of Exploration Geophysicists*. June.

Xiaobing Z. 2009. 3D vector gravity potential and line integrals for the gravity anomaly of a rectangular prism with 3D variable density contrast. *Geophysics*; 74(6):I43–I53.

Zhdanov MS, Wilson GA, Xiaojun L. 2010. 3D imaging of subsurface structures using migration and regularized focusing inversion of gravity and gravity gradiometry data. *Airborne Gravity* - Abstracts from the ASEG-PESA Airborne Gravity Workshop, *Geoscience Australia Record*; 23.